Available online at www.sciencedirect.com
SCIENCE DIRECT®

Journal of the European Ceramic Society 24 (2004) 2657–2667
www.elsevier.com/locate/jeurceramsoc

Modelling of thermal conductivity of porous materials: application to thick thermal barrier coatings

F. Cernuschi[a,*], S. Ahmaniemi[b], P. Vuoristo[c], T. Mäntylä[c]

[a]*CESI S.p.a., Via Reggio Emilia, 39, 20090 Segrate (MI), Italy*
[b]*Metso Paper Inc, PO Box 587, FIN-40101, Jyväskylä, Finland*
[c]*Tampere University of Technology, Institute of Materials Science, PO Box 589, 33101 Tampere, Finland*

Received 27 March 2003; received in revised form 2 September 2003; accepted 6 September 2003

Abstract

Modelling of thermal conductivity of two and three phase composite materials is used to determine the thermal conductivity of thick porous zirconia based thermal barrier coatings for use in high temperature applications. These coatings, depending on the deposition technique and process parameters exhibit different degrees of porosity. The porosity of the coating has an affect on thermal properties in completely different ways depending on the morphology and the orientation of the pores dispersed within a continuous matrix. In this work air plasma sprayed coatings have been considered. The experimental results were successfully compared to the modelled thermal conductivities. In the model the effects of porosity were taken into account considering the shape, orientation and volumetric percentage of pores. Image analysis and mercury porosimetry was used in experimental porosity determination.

Keywords: Functional applications; Plasma spraying; Porosity; Thermal barrier coatings; Thermal conductivity; ZrO_2

1. Introduction

Thermal conductivity plays a key role in heat transfer processes. As a matter of fact in many industrial applications, materials are selected primarily by considering their mechanical and thermal properties. In aerospace, power generation and automotive industries, materials like metal or ceramic matrix composites and porous ceramic thermal barriers are widely used for manufacturing the most advanced components. In particular, the last generation hot path components of gas turbines (typically combustion chambers, transition pieces, turbine blades and vanes) are protected against hot gases (>1300 °C) by ceramic thermal barrier coatings (TBCs). In practice the thickness of TBCs is in the range of 300–1000 μm.

There have been high expectations of using TBCs also in diesel engines. With TBCs the mean combustion temperature could be increased in the diesel process. At the same time the heat losses to the cooling system could be decreased. This extra heat could be recovered in a turbocharger or in a flue gas boiler in a combined cycle. Some studies have shown that TBCs can increase the coefficient of thermal efficiency of diesel process and lower the fuel consumption.[1] Emissions such as NO_x, SO_x, CO, CO_2, unburned hydrocarbons and particle emissions have been studied in engine tests with and without TBCs.[1–3] Most of these studies disclose that TBCs decrease the fuel consumption, but have a minor effect on emissions. Without question the diesel process has to be adjusted correctly to utilise the benefits of thermal barrier coating.

Porous TBC's can drastically reduce the temperature by 100–300 °C of the internally cooled metallic base materials, depending on the coating thickness and microstructure. The selection of the best insulating coating significantly increases the efficiency of the gas turbine because either the cooling flow can be reduced or a higher turbine inlet temperature (TIT) can be achieved.[4] Thermal properties of TBCs, apart from the intrinsic thermal properties of the coating material, depend on the deposition technique used and the

* Corresponding author. Tel.: +39-22-125-8740.
E-mail addresses: cernuschi@cesi.it (F. Cernuschi).

0955-2219/$ - see front matter © 2003 Elsevier Ltd. All rights reserved.
doi:10.1016/j.jeurceramsoc.2003.09.012

Nomenclature

f_i	volumetric fraction of the i-th phase of a composite. f ranges from 0 up to 1
Matrix	a continuous homogeneous media within which, a dispersion of an other material in form of particles can be embedded
Ellipsoid	a solid surface whose generic point p = p(x, y, z) satisfies the equation $\frac{x^2}{a^2}+\frac{y^2}{b^2}+\frac{z^2}{c^2}=1$ where a, b, c represent the lengths of the three mutually perpendicular axes of this solid
Spheroid	ellipsoids having a revolution axis corresponding to the ellipsoid axis a and thus with the other two axes equal i.e. $b=c$
Shape factor F	a numerical value related to the shape of the spheroid
X factor	a numerical value taking into account both the shape and the orientation of a spheroid in respect to a uniform field (i.e. heat flux)
d	dimension of the considered euclidean space (typically 3)
Fractal dimension D	it is a positive real number representing the degree of irregularity and discontinuance of an object which has the self-similarity property
k	the thermal conductivity of a composite
k_i	the thermal conductivity of the i-th phase of a composite material
k_m	the thermal conductivity of the matrix of a composite material
k_d	the thermal conductivity of the dispersed phase d of a composite material
δ	thickness of lamellae constituting a TBCs'
φ	fraction of the total area where the true contact between two layers of a TBCs' coating deposited by air plasma spray is guaranteed because no pores are in between. This numerical value ranges from 0 up to 1
Φ, Θ and Φ	functions each representing the effect of a different type of porosity on the thermal conductivity of a porous material in Eqs. (14) and (15). In particular, in the frame of this work Ψ, Θ and Φ refer to penny shape, not flat spheroidal and open porosity respectively

process parameters. These factors affect on the content, the shape and the orientation of porosity inside the TBC.

As the high temperature performance of TBC structures is strongly related to the porosity features, it is important to be able to a priori design the thermal properties of these materials as well as to theoretically interpret the experimental results. These two tasks can be faced easier if reliable modelling of thermal properties of TBCs can be done. The models also should take into account the shape, orientation and the volumetric percentage of the porosity. In the following chapter a short review of modelling of thermal conductivity of two-phase systems is presented (i.e. ceramic matrix and the pores in TBC, metallic/ceramic matrix and the reinforcement in composites, etc.). The latter part of this paper concentrates on the specific case of porous TBCs.

2. Thermal conductivity of a two-phase composites

The in-serie and in-parallel models proposed by Voigt-Reuss are the simplest models which give the two extreme limits for the thermal conductivity of a two-phase composite.[5] This model describes a composite, constituted of an alternate sequence of layers of two phases. Depending on the disposal of layers in respect to the heat flux direction, the series or parallel scheme is obtained.

Generally, almost all the models proposed in the literature could be classified into asymmetrical or symmetrical, depending on the schematisation of the roles of the different phases. A two-phase composite material could be described as constituted either by a dispersion of isolated grains embedded within a continuous matrix or by a symmetrical penetration of grains of the two phases occupying the whole volume.

2.1. Asymmetrical models

Many asymmetrical models have been proposed after the pioneering studies of Maxwell[5] and Rayleigh.[6] In particular, the Maxwell model is applicable only for a very diluted (volumetric fraction below 10%) dispersion of spheres within a continuous matrix because he assumed that the field was one-dimensional at a sufficiently long distance from each sphere.

If k_m, k_d and f are the thermal conductivities of the matrix and of the dispersed spheres and the dilute volumetric fraction respectively, expanding the Maxwell solution in a Taylor series about $=0$, the thermal conductivity k of the composite can be written as:

$$\frac{k}{k_m} = 1 - \left[\frac{3f(1 - k_d/k_m)}{\left(2 + \frac{k_d}{k_m}\right)} \right] \tag{1}$$

Subsequently the Maxwell model was also extended to consider a dilute consisting of a dispersion of randomly oriented ellipsoidal particles.[7]

A significant improvement to asymmetrical modelling was given by Bruggeman who in fact assumed that the sphere radius of the dilute dispersion varied within an infinite range of values and that each single sphere was embedded within the continuous matrix.[8] Starting from these assumptions he showed that the limitation on the volumetric fraction of the dilute dispersion can be removed (i.e $0 \leqslant f < 1$). In this case the equation derived is:[9,10]

$$\frac{\left(k/k_m - \frac{k_d}{k_m}\right)}{\left[\left(\frac{k}{k_m}\right)^{1/3}\left(1 - \frac{k_d}{k_m}\right)\right]} = 1 - f \tag{2}$$

Also in this case, analogously to the Maxwell model, it is possible to generalise the modelling to a solute dispersion of randomly oriented ellipsoids.[11–13]

Of particular interest is the specific case of spheroids (ellipsoids having a revolution axis corresponding to the ellipsoid axis a and thus with the other two axes equal i.e. $b=c$) because a wide interval of real situations can be modelled by defining an orientation angle α between the field gradient (the heat flux) and the dispersed particles and by varying the ratio a/c between the two axes of the spheroid.

Considering further models proposed in the literature, the Meredith and Tobias model was well suited to dilute dispersions with a particle size distribution not wide as required by the Bruggeman model. The limitation to volumetric fractions <0.6 is the main drawback of this model[10]

2.2. Symmetrical models

As previously described, in symmetrical models the two phases (named 1 and 2) play interchangeable roles. To make more evident this symmetry, the thermal conductivity and the volumetric fractions of both phase 1 and phase 2 are indicated as k_1, k_2, f_1 and f_2 (where obviously $f_2 = 1 - f_1$). In particular, if both phases consist of spheres of a very wide size range, the following equation could be used:[14–16]

$$\frac{f_1(k_1 - k)}{[k_1 + (d-1)k]} + \frac{f_2(k_2 - k)}{[k_2 + (d-1)k]} = 0, \tag{3}$$

where d is the space dimension (typically 3). Also this model can be extended to randomly oriented ellipsoids.[17]

3. Modelling for porous materials

For porous materials like a TBC, the thermal conductivity of pores can be assumed to be negligible (i.e. k_d or $k_i \cong 0$). In particular, this is true for temperatures where inside the pores the radiative contribution to the thermal conductivity of the composite can be neglected. So all the models are significantly simplified and they can be applied in semi-quantitative explanation of the experimental results related to thermophysical and microstructural characterisation[18–21] as also shown in this study. With this assumption, the two extreme limits of the thermal conductivity, as determined by Voigt-Reuss, are:[7]

$$0 \leqslant k \leqslant (1 - f)k_m \tag{4}$$

3.1. Asymmetrical models

The Maxwell and the Bruggeman models represented by Eqs. (1) and (2) respectively become:[10,13,14]

$$\frac{k}{k_m} = \left(1 - \frac{3}{2}f\right) \tag{5}$$

$$\frac{k}{k_m} = (1 - f)^{\frac{3}{2}} \tag{6}$$

More generally, for a dispersion of spheroids, the Bruggeman model is:[13]

$$\frac{k}{k_m} = (1 - f)^X \tag{7}$$

where $X = \frac{1-\cos^2\alpha}{1-F} + \frac{\cos^2\alpha}{2F}$, in which F is the shape factor of the spheroid, and α is the angle between the revolution axis of the spheroid and the non perturbed heat flux.[12, 22] Fig. 1 graphically represents the value of the shape factor F as a function of the axial ratio a/c. In particular, for sphere ($a=c$) F is 1/3 while for oblate ($c>a$) and prolate ($a>c$) spheroids F values are in the range of 0–1/3 and 1/3–1/2, respectively. Fig. 2 shows the X values for three different cases. In particular, for lamellar porosity ($c>a$) the X factor gets very high values when the a axis is either randomly oriented or parallel to the heat flux. On the contrary, if lamellae are oriented normal to the heat flux, X is equal to 1. For cylinders, X values tend to be 1, 1.667 or 2 depending if

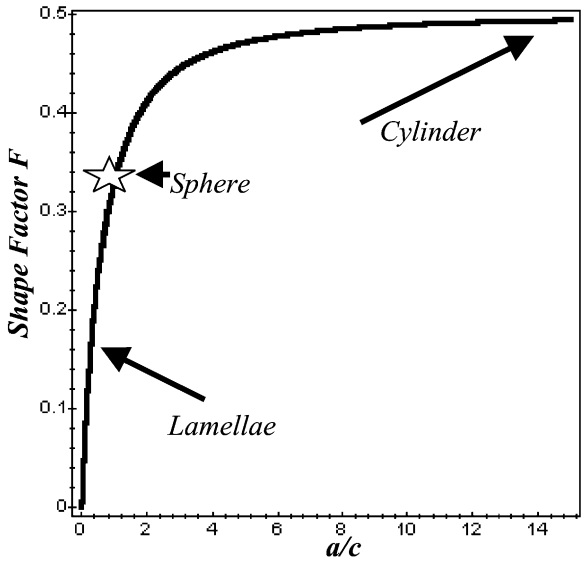

Fig. 1. Shape factor F as a function of the axial ratio a/c of the spheroid.

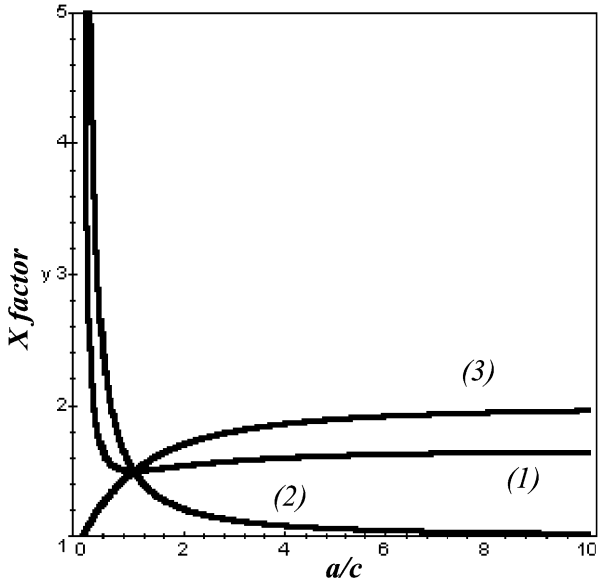

Fig. 2. X factor as a function of the axial ratio a/c of the spheroid for (1) randomly oriented spheroids, (2) spheroids oriented with the revolution axis a parallel to the heat flux (i.e. $\cos^2\alpha = 1$), and (3) spheroids oriented with the revolution axis a normally to the heat flux (i.e. $\cos^2\alpha = 0$). The crossing point of these curves refers to the sphere (i.e. $a/c = 1$, X = 1.5).

the a axis is parallel, randomly oriented or perpendicular respectively.

From the previous considerations it is clear that Eq. (7) is well suited to describe a wide range of closed porosity configurations in term of voids shape and orientation. Moreover Schulz showed that also randomly oriented open porosity can be accurately described by Eq. (7).[13] Furthermore, it is interesting to observe that for spheres, this equation reduces to Eq. (6) which expanded in Taylor series close to zero becomes equal to

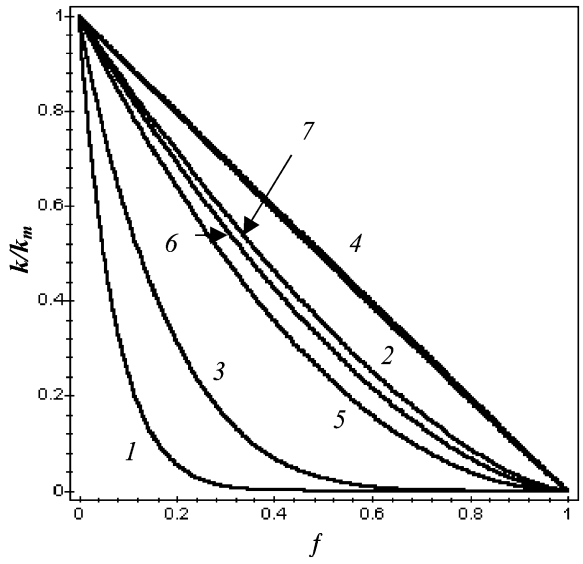

Fig. 3. The ratio $\frac{k}{k_m}$ vs. the volumetric fraction of porosity as estimated by Eq. (7) for lamellae ($F = 0.0369$) with the revolution axis (1) parallel, (2) perpendicular and (3) randomly oriented and for cylinders ($F = 0.499$) with the revolution axis (4) parallel, (5) perpendicular, (6) randomly oriented to the heat flux and for (7) spheres.

Eq. (5). Fig. 3 shows the ratio $\frac{k}{k_m}$ as a function of the volumetric fraction of porosity as described for pores of different shape and orientation in respect to the heat flux by the Bruggeman model. In particular a small amount of lamellar (penny shaped) pores with the major axis oriented parallel to the heat flux produces a strong reduction of the thermal conductivity of the porous material. A similar result was obtained by Hasselman who described the effect of penny shaped pores on the thermal conductivity starting from the extension to revolution ellipsoids of the Maxwell model.[18]

The extension of the Meredith and Tobias model to the case of randomly oriented spheroidal porosity gives:[10]

$$\frac{k}{k_m} = \left[\frac{2-f}{2+(W-1)f}\right]\ \left[\frac{2(1-f)}{2(1-f)+Wf}\right], \tag{8}$$

where $W = \frac{1}{3}\left(\frac{1}{2F} + \frac{2}{(1-F)}\right)$ that is the X factor for randomly oriented spheroids.

A comparison between the models of Voigt-Reuss, Maxwell, Bruggeman and Meredith and Tobias have been considered in Fig. 4 for randomly oriented spheroids with the shape factor $F = 0.1$. As expected, the Voigt-Reuss model describes the two extreme limits of variability of the ratio $\frac{k}{k_m}$ while the Meredith and Tobias model represents an intermediate situation between Maxwell and Bruggeman models. As the Bruggeman model appears to be able to describe the widest range of situations, it will be applied to the selected specific experimental cases in the following.

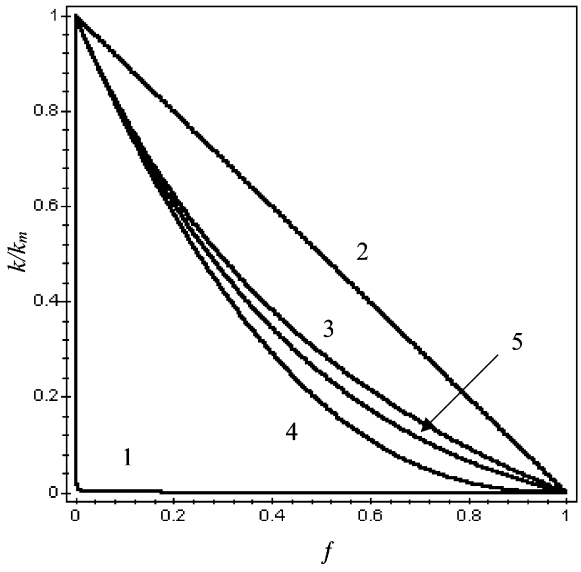

Fig. 4. The ratio $\frac{k}{k_m}$ vs. the volumetric fraction of porosity as estimated by Voigt-Reuss (1) in serie and (2) in parallel models. (3) Maxwell, (4) Bruggeman and (5) Meredith and Tobias models for a randomly oriented lamellar porosity with a shape factor $F=0.1$.

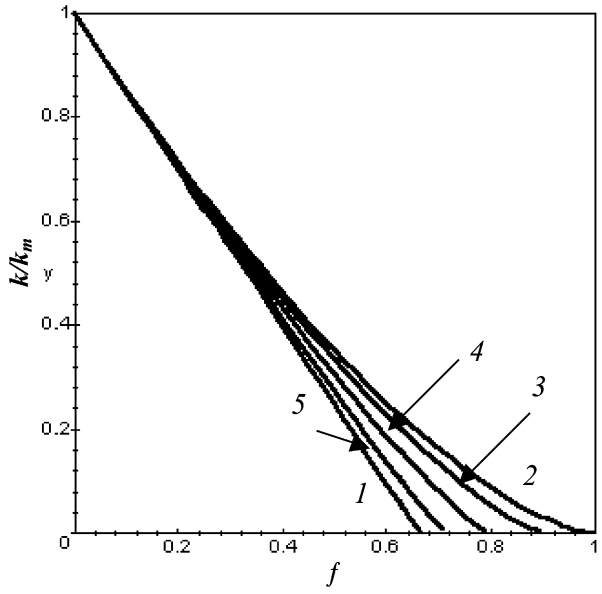

Fig. 5. The ratio $\frac{k}{k_m}$ vs. the volumetric fraction of porosity as estimated by Eq. (11) for (1) symmetrical limit $D=3$, (2) asymmetrical limit $D=2$ and for fractal dimension (3) $D=2.2$, (4) $D=2.5$ and (5) $D=2.8$.

3.2. Symmetrical models

For a symmetrical porous material (i.e. $k_1 \cong 0$) Eq. (3) simplify as follows:

$$\frac{k}{k_2} = \left(1 - \frac{3}{2}f\right) \tag{9}$$

The main result is that this equation corresponds to Eq. (5) obtained for the Maxwell asymmetrical model restricted to a very diluted dispersion. This means that under peculiar conditions (very diluted not conducting sphere dispersion) the two approaches converge to the same formulas.

Furthermore, for a symmetrical dispersion of two sets of spheroids where one of them consists of pores (i.e. $k_1 \cong 0$), Eq. (3) generalises as follows:[17]

$$\frac{f_1 k}{[(1-F_1)k]} = \frac{f_2(k_2-k)}{[F_2 k_2 + (1-F_2)k]} \tag{10}$$

where F_1 and F_2 are the shape factors for the two spheroidal dispersions.

3.3. Other models

Both asymmetrical and symmetrical models assumed well defined configurations of the porosity (i.e. dispersion of spheroids in a continuous matrix or in spheroids), but in some cases, the reality should be represented by an intermediate situation. McLachlan proposed a model introducing the idea of a conducting-insulating transition. More in details, looking at the Eqs. (6) and (9) for the three dimensional space, the conducting- insulating transition takes place for the critical values $f=1$ and $f=2/3$ respectively. More generally for a space of d dimensions, the critical value of the volumetric fraction equal to $\frac{(d-1)}{\mathrm{d}}$. Starting from this analysis, McLachlan proposed the phenomenological equation:[23]

$$\frac{k}{k_m} = \left[1 - \frac{f}{f_c}\right]^{df_c/(d-1)} \tag{11}$$

where $f_c = \frac{(d-1)}{D}$ and D is the fractal dimension of the system. In particular D is a positive real number representing the degree of irregularity and discontinuance of an object which has the self-similarity property.[24–26] In this specific contest, the two limit values of D are $D=d$ (symmetrical model) and $D=d\text{-}1$ (asymmetrical model) but D can assume also intermediate values depending on the specific real case. Furthermore, a possible generalisation of Eq. (11) to spheroids derived from Eq. (7) is:[23]

$$\frac{k}{k_m} = \left[1 - \frac{f}{f_c}\right]^{f_c X} \tag{12}$$

Fig. 5 graphically represents the ratio $\frac{k}{k_m}$ vs. volumetric fraction of porosity as described by Eq. (11) for different values of the parameter D. As expected, depending to the fractal dimension D, the transition conducting–insulating takes place at different values.

Another model, specifically proposed by McPherson[27] for ceramic TBC, deposited by air plasma spray (APS), yields the similitude between the electrical resistance of metallic contacts and the heat flux. The model is restricted to conduction through the various points of true contact between lamellae to determine the ratio between the thermal conductivity of bulk and the porous materials.

In particular, on the basis of microstructural observations with transmission electron microscopy (TEM), the porosity was assumed to consist of circular microcracks parallel to the coating surface. Microcracks were distributed in planes mutually separated just by the thickness δ of the lamellae. If φ is the fraction of the apparent area of the true contact on each plane, the ratio between the through-the-thickness thermal conductivity of porous and bulk material is:[27]

$$\frac{k}{k_m} = \frac{2\varphi\delta}{\pi a} \tag{13}$$

where a is the radius of each true contact circular area. In the specific case considered by McPherson, the $2a$ diameter and the lamellar thickness δ were comparable. This model has been suitably modified also for taking into consideration the gas present within the pores as well as the radiative contributions at high temperature.[27]

3.4. Extension to models for composites containing many porosity types

All the models previously described assume the porosity consisting of single shape pores or cracks having also a single orientation. Nevertheless, the porosity of a real TBC (typically deposited by APS) is a mixture of different type of pores. Thus, the modelling of real cases could require the superimposition of the contributions of different porosity types to the overall thermal conductivity of the porous material.

A possible approach to extend these models to a manifold porosity system consists in applying in an iterative way a two-phase modelling.[20,21,28] In particular if f_0 is the total amount of porosity and f_1 and f_2 are the percentages of the types of porosity respectively ($f_0 = f_1 + f_2$), the thermal conductivity of the three-phase mixture is:

$$\frac{k}{k_m} = \frac{1}{2}\left\{\Phi\left[\frac{f_2}{(1-f_1)}\right]\Psi(f_1) + \Psi\left[\frac{f_1}{(1-f_2)}\right]\Phi(f_2)\right\} \tag{14}$$

where $\Psi(f)$ and $\Phi(f)$ indicate are the functions describing the effect of porosity on the thermal conductivity of the matrix. In particular, Ψ and Φ can be chosen between the different expressions previously defined depending on the morphology of the porosity which has be modelled.

This iterative approach to extend models developed for a material containing a single type of porosity (for example spheres) to materials containing many types of porosity (for example spheres, cylinders and lamellae) is an hybrid between symmetrical and asymmetrical approaches. In fact, the addition of the first porosity to a continuous matrix requires to use an asymmetrical model but for the subsequent iterations, needed to take into account the other porosity types, the matrix could not be considered exactly continuous anymore because of the presence of the first dispersion. However, the result for the special case $\Phi(f) \equiv \Psi(f) = (1-f)^X$ (corresponding to account for a given amount of porosity of a single type using the proposed iterative approach) Eq. (16) reduces to Eq. (9) giving indications that this approach could be applied for extending the Bruggeman asymmetrical model from a single shape porosity to a spectrum of different porosity shapes if, for each porosity type, the size of the dilute dispersion varies within a very wide range of values.

Thus, when a higher number of porosity types should be simultaneously considered (for example three), it is sufficient to apply the iterative procedure ones more. In particular, if f_3 and $\Theta(f)$ are the volumetric fraction and the function describing the contribution of the third porosity type to the thermal conductivity respectively, the expression giving the final thermal conductivity k of the four phase system is:

$$\begin{aligned} k = \frac{k_0}{6}\Bigg\{ & \Phi\left[\frac{f_2}{(1-(f_1+f_3))}\right]\Psi\left(\frac{f_1}{(1-f_3)}\right)\Theta(f_3) \\ & + \Psi\left[\frac{f_1}{(1-(f_2+f_3))}\right]\Phi\left(\frac{f_2}{1-f_3}\right)\Theta(f_3) \\ & + \Phi\left[\frac{f_2}{(1-(f_1+f_3))}\right]\Theta\left(\frac{f_3}{1-f_1}\right)\Psi(f_1) \\ & + \Psi\left[\frac{f_1}{(1-(f_2+f_3))}\right]\Theta\left(\frac{f_3}{1-f_2}\right)\Phi(f_2) \\ & + \Theta\left(\frac{f_3}{(1-(f_1+f_2))}\right)\Phi\left[\frac{f_2}{1-f_1}\right]\Psi(f_1) \\ & + \Theta\left(\frac{f_3}{(1-((f_1+f_2))}\right)\Psi\left[\frac{f_1}{(1-f_2)}\right]\Phi(f_2)\Bigg\} \end{aligned} \tag{15}$$

The peculiar structure of Eqs. (14) and (15) has been defined in order to obtain expressions independent from the order of mixing the different porosity types within the matrix.

4. Application to selected real cases of porous TBC

As described in details elsewhere,[29,30] the measurements of thermal conductivity on some different TBC have been carried out: in particular, thick zirconia based TBC stabilised by three different oxides ($8Y_2O_3ZrO_2$, 22 wt.%MgO–ZrO_2, and 25 wt.%CeO_2–2.5Y_2O_3–ZrO_2). In order to detect, if present, any densification process caused by the high temperature exposure during the measurement itself, the thermal conductivity has been

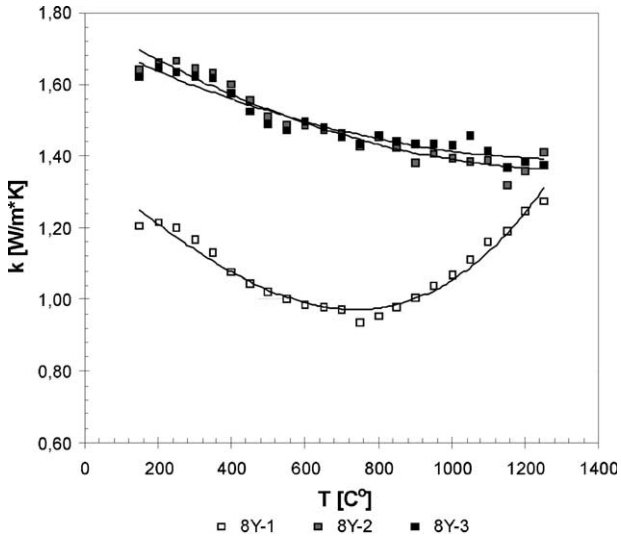

Fig. 6. Thermal conductivity of $8Y_2O_3$–ZrO_2 coating as measured during the first, second and third cycle.

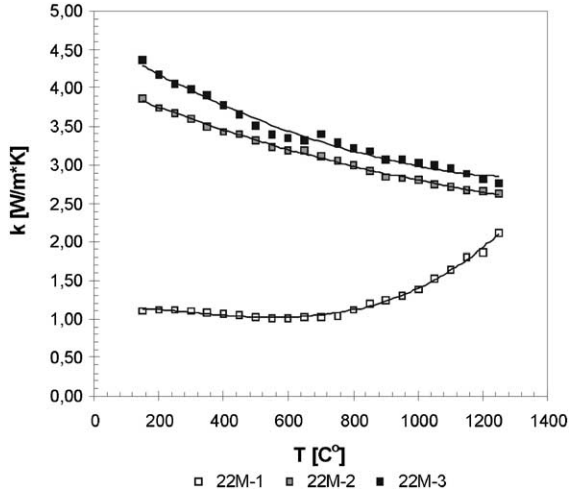

Fig. 7. Thermal conductivity of $22MgO$–ZrO_2 coating as measured during the first, second and third cycle.

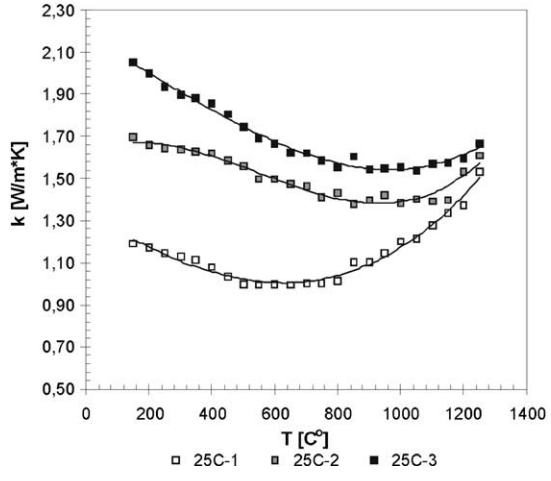

Fig. 8. Thermal conductivity of $25CeO_2$–$2.5Y_2O_3$–ZrO_2 coating as measured during the first, second and third cycle.

evaluated at temperatures within the range (150–1250 °C) and each measurement cycle has been repeated three times as shown by Figs. 6–8. Table 1 reports the values of sample thickness as measured by optical microscopy in 25 different position all along the sample section.

Before and after the thermal conductivity measurements, the evaluation of the porosity by image analysis (IA) and mercury intrusion porosimetry (MIP) has been performed. Moreover microstructural characterisation by optical microscopy and SEM has also been carried out. Characterization studies confirmed that some irreversible microstructural changes took place during the exposure to high temperature.[29,30] In particular, reduction of the crack-like micro-porosity has been observed due to the densification processes, typically caused by sintering. These could be considered as the main mechanisms causing the increase of thermal conductivity as pointed by microstructural analysis.[30] Moreover, for thick TBC an other possible contribution to the increase of thermal conductivity could be ascribed to changes of the pore structure caused by the residual stress relaxation at high temperature as reported by Schwingel et al.[31] even if in this specific case, no clear evidence of any significant stress relaxation has been observed during specific heat measurements.[30]

In order to explain semi-quantitatively the thermal conductivity variations observed between the first and the third cycle for the three as-sprayed samples, modelling for porous materials was applied using IA and MIP results as input data. As a matter of fact, most of the models require the volumetric fraction, the shape and orientation distribution of pores. But both measurement techniques, IA and MIP, have some limitations. In fact, the latter technique allows estimating only the open porosity content and pores are assumed cylindrical shaped.

On the contrary, IA can estimate the overall porosity content, but sample preparation could limit the precision because of the creation of artefacts. Fortunately, this effect can be significantly reduced by using an under vacuum sample impregnation procedure and a suitable sample polishing. Moreover, to correctly evaluate the shape and the size distribution of voids inside a porous sample, IA should require a stereological interpretation of cross-section analysis.

The most reliable void distribution would be obtained by applying the small angle neutron scattering (SANS)

Table 1
Summary of experimental results

Sample	Composition	Treatment	Thickness [μm]
8Y PSZ	Y_2O_3 8 wt.%	As sprayed	796±20
22MSZ	MgO 22 wt.%	As sprayed	940±14
25CSZ	CeO_2 25 wt.%	As sprayed	985±14

to TBC, but ones requires the access to a dedicated neutron facility and it is also very time consuming.[32]

By observing SEM micrographs (see Figs. 9 and 10), as also suggested in the literature, porosity could be classified in:[33–36]

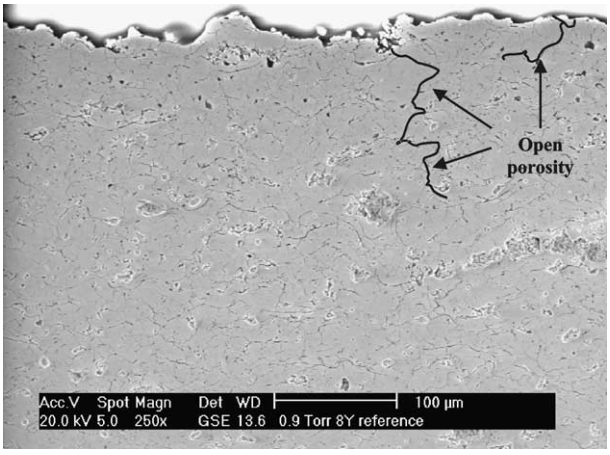

Fig. 9. SEM micrograph of the $8Y_2O_3$–ZrO_2 coating showing the typical microstructure of the plasma sprayed coating. The arrows show an example of a net of open pores.

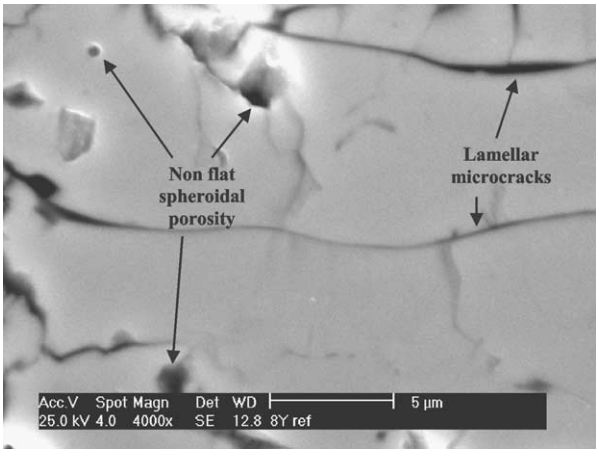

Fig. 10. High magnification SEM micrograph of the $8Y_2O_3$–ZrO_2 coating. Arrows show lamellar microcracks and non flat spheroidal pores.

- Inter- intra- and trans-lamellar microcracks with the smaller axis typically oriented parallel (inter-lamellae) and perpendicular (intra- and trans-lamellae) to the heat flux (i.e. through-the-thickness of the TBC);
- non flat spheroidal porosity; and
- randomly oriented open porosity.

In order to semi-quantitatively explain the experimental results, closed porosity fraction was assumed as the difference between the total porosity measured by IA and the total open porosity estimated by MIP.

At high temperatures the narrowest microcracks have a large affect on the increase of thermal conductivity. The reason for that is that the improved lamellae contact, caused by sintering phenomena, is more probable within the narrow sized microcracks. However, it was very difficult to classify the size of microcracks for the modelling purposes, but as a first attempt the upper limit of 100 nm for the narrow type of microcracks was arbitrary chosen. At the same time the remnant fraction of open porosity (the range >100 nm in MIP analysis) was considered as open randomly distributed porosity.

For the computation of the thermal conductivity both before and after the measurement cycles, Eq. (15) has been used where the Ψ, Φ and Θ functions are all defined by Eq. (7). In particular, microcracks (function Ψ) could be described by sharp disk shaped spheroids (penny shaped pores). Starting from the observations of TBC sections, the orientation of microcracks appears to have a bimodal distribution. In fact, two main orientations for the penny shaped cracks can be observed. The main fraction (hereinafter fixed equal to 75%) has the revolution axis parallel to the coating thickness while the remnant part (25%) has the revolution axis oriented perpendicularly to the heat flux.

Thus, following literature data,[33,35] the average ratio c/a for penny shaped microcracks has been reasonably chosen equal to 15. For non flat spheroids (function Θ) with the revolution axis parallel oriented to the heat flux, the ratio c/a was fixed equal to 3, corresponding to a final X factor $=1.7$. The open randomly oriented

Table 2
Input parameters for modelling

Sample	Bulk thermal conductivity [W/mK]	Overall porosity (IA)		Open randomly oriented porosity (MIP > 100 nm)		Microcracks (MIP < 100 nm)		Non flat porosity (IA-MIP)	
		Before H.T.	After H. T.	Before H.T.	After H. T.	Before H.T.	After H. T.	Before H.T.	After H. T.
8YPSZ	2.8	24.9	19.7	0.9	5.2	9.4	2.8	14.6	11.7
22MSZ	2.2	16.4	15.1	4.5	10.4	5	3.3	6.9	1.4
25CSZ	2.8	18.7	13.9	3.9	1	6.5	7.5	8.3	5.4

Table 3
Comparison between the experimental thermal conductivity data and the results of the simulations

Sample	Experimental thermal conductivity [W/m°C]		Simulated thermal conductivity [W/m°C]	
	Before H.T.	After H. T.	Before H.T.	After H. T.
8YPSZ	1.2	1.62	1.00	1.68
22MSZ	1.1	4.37	1.2	1.37
25CSZ	1.19	2.05	1.13	1.68

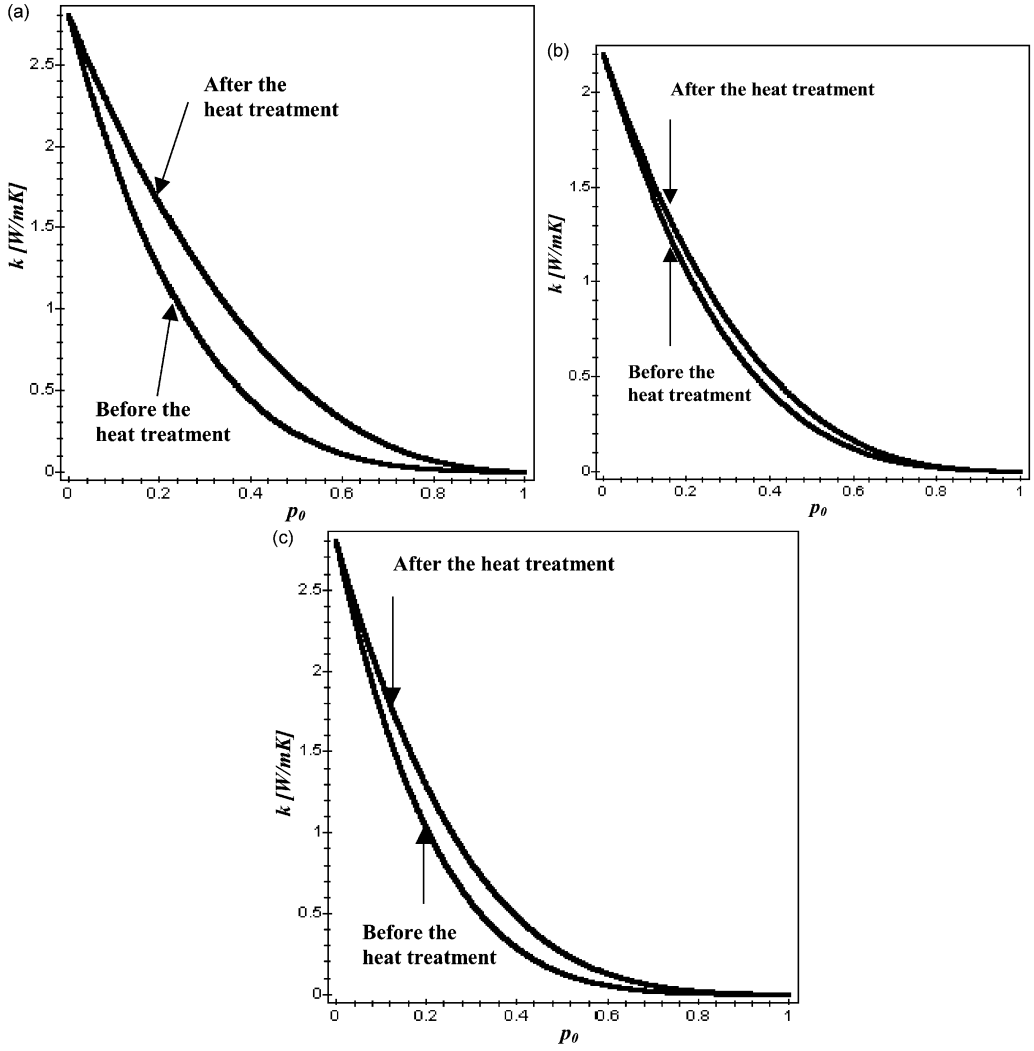

Fig. 11. Thermal conductivity as a function of the overall porosity content f_0 (with relative percentages of the different porosity types as specified within Table 2) for (a) $8Y_2O_3$–ZrO_2, (b) 22MgO–ZrO_2 and (c) $25CeO_2$–$2.5Y_2O_3$–ZrO_2. For each of the three cases, the lower and the upper curves refer to the porosity distribution before and after the heat treatment respectively. The arrows indicate the points (see Table 3) on the two curves corresponding to the experimental porosity levels (see Table 2).

porosity (Φ function) can be described choosing the X factor equal to 1.66 as pointed out by Schulz.[13]

Since the penny shaped cracks are oriented along two different directions, in order to apply the model, some additional calculations are required. In fact, the Eq. (15) should be extended from three up to four porosity types increasing the number of terms of the equation from 6 up to 24. An alternative solution consists in solving the following Eq.:

$$\frac{1}{2}\left\{\left[1-\frac{f_2}{(1-f_1)}\right]^{X_2}(1-f_1)^{X_1} + \left[1-\frac{f_1}{(1-f_2)}\right]^{X_1}(1-f_2)^{X_2}\right\} = (1-f)^X, \tag{16}$$

where f, f_1, f_2 are the total amount, the parallel and the perpendicular fractions of microcrack-type of porosity respectively and X is the exponent related to an "effective" factor for the mixture of parallel and perpendicular microcracks in the percentages as defined by f_1, f_2 and characterised by the factors X_1 and X_2 respectively.

If considering the bulk thermal conductivity of the studied samples and the relative percentages of open, closed and microcracks porosity both before and after the thermal cycling, two decreasing curves describing the thermal conductivity as a function of the porosity percentage can be obtained.

Table 2 resumes the input data of the model for the three samples considered while Table 3 and Fig. 11 summarise the results of these computations. The experimental thermal conductivity has been considered at the lowest measuring temperature (150 °C), because the porosity data refers to the measurements carried out at RT. Furthermore at low temperatures, the radiative contribution to the heat transmission through the pores can be neglected as assumed in this modelling.

It is interesting to observe how the results of computations agree quite satisfactory with all the experimental data apart the heat treated 22MgO–ZrO_2 sample. This can be explained due the fact that phase changes (c/t-ZrO_2 to m-ZrO_2) took place in 22M coating. The phase change was caused by unstabilization of the 22MgO–ZrO_2 material. MgO precipitated from the zirconia matrix in the first run at 1000–1250 °C as described in details elsewhere.[29,30] Thermal conductivities of m-ZrO_2 and MgO are much higher if compared to the partially stabilized zirconia, so for that reason there was a gap between the measured and modelled results.

5. Conclusions

Starting from the general purpose Bruggeman model for thermal conductivity in an asymmetrical two phase composite, the specific cases of three zirconia based porous TTBC have been studied. In particular, the model has been extended to a four-phase system by an iterative approach in order to describe the three different classes of porosity (closed non flat spheroids, open randomly oriented porosity and microcracks) identified within the TBC by microstructural analysis and proposed in the literature. Notwithstanding some hypotheses and simplifications have been required in order to perform computations, the results of these simulations show a good agreement with the experimentally measured thermal conductivity for samples where no other reactions different from densification take place during the high temperature exposure. To increase the precision and the reliability of the modelling, further microstructural studies to more precisely characterise pores in term of true shape, orientation distribution and spheroid aspect ratio c/a are required.

Acknowledgements

This study has been partially conducted within the frame of "Ricerca di Sistema" D.L. MICA 26/01/2000.

References

1. Swaminathan, V. P. and Cheruvu, N. S., Gas turbine hot-section materials and coatings in electric utility applications. In *Advanced Materials and Coatings for Combustion Turbines*, ed. V. P. Swaminathan and N. S. Cheruvu. ASM International, Materials Park, OH-USA, 1994.
2. Parker, D. W., Thermal barrier coatings for gas turbines, automotive engines and diesel engines. *Materials & Design*, 1992, **13**(6), 345–351.
3. Winkler, M. F. and Parker, D. W., Thermal barrier coatings for diesel engines—ten years of experience, *SAE Technical Paper Series*, No 922438, 1992.
4. Osawa, K., Kamo, R. and Valdmanis, E., Performance of thin thermal barrier coating on small aluminum block diesel engine, *SAE Technical Paper Series*, No: 910461, 400 Commonwealth Drive, Warrendale, Pa. 15096-0001, USA, 1991.
5. Maxwell, J. C., *A Treatise on Electricity and Magnetism*, 2nd ed., Vol. 1. Clarendon Press, Oxford, 1881.
6. Lord Rayleigh, On the influence of obstacles arranged in rectangular order upon the properties of a medium. *Phil. Mag*., 1892, **34**, 481.
7. Grimvall, G., *Thermophysical Properties of Materials. Selected Topics in Solid State Physics. Vol. XVIII*. North-Holland Physics Publishing, 1986.
8. Fricke, H., A mathematical treatment of the electric conductivity of disperse systems: the electric conductivity of a suspension of homogeneous spheroids. *Phys. Rev*., 1924, **24**, 575.
9. Bruggeman, D. A. G., Berechnung verschiedener physikalischer Konstanten von heterogenen Substanzen. *Ann. Physik*, 1935, **24**, 636.
10. Meredith, R. E. and Tobias, C. W., Conduction in heterogeneous systems. In *Advances in Electrochemistry and Electrochemical Engineering, Vol. 2*, ed. C. W. Tobias. Interscience, New York, 1962, pp. 15.
11. Meredith, R. E., Studies in the conductivities of dispersions, *Lawrence Radiation Laboratory Report, UCRL-8667*, 1959.
12. Schulz, B., Die Abhangigkeit der Feldeigenschaften zweiphasiger Werkstoffe von ihrem Gefuegeaufbau. Theoretische Uberlegungen und experimentelle Prufung am Beispiel der Warmleitfahigkeit von Cermets, *Report KfK 1988*, Kernforschungszentrum Karlsruhe, FRG 1974.
13. Schulz, B., Thermal conductivity of porous and highly porous materials. *High Temp. High Press*., 1981, **13**, 649.
14. McLachlan, D. S., Equation for the conductivity of metal-insulator mixtures. *J. Phys. C: Solid State Phys*, 1985, **18**, 1891.
15. McLachlan, D. S., An equation for the conductivity of binary mixtures with anisotropic grain structures. *J. Phys. C: Solid State Phys*, 1987, **20**, 865.
16. Brailsford, D. and Major, K. G., The thermal conductivity of aggregates of several phases, including porous materials. *Brit. J. Appl. Phys*., 1964, **15**, 313.
17. Bjorneklett, A., Haukeland, L., Wigren, J. and Kristiansen, H., Effective medium theory and the thermal conductivity of plasma-sprayed ceramic coatings. *J. Mater. Science*, 1994, **29**, 4043.
18. Hasselman, D. P., H, Effect of cracks on thermal conductivity. *J. Comp. Mater*., 1978, **12**(19), 403–407.
19. Litovsky, E.Ya. and Shapiro, M., Gas pressure and temperature dependances of thermal conductivity of porous ceramic materi-

als: part 1, refractories and ceramics with porosity below 30%. *J. Am. ceram. Soc.*, 1990, **75**, 3425.
20. Cernuschi, F., Bianchi, P., Leoni, M. and Scardi, P., Thermal diffusivity/microstructure relationship in Y-PSZ thermal barrier coatings. *Journal of Thermal Spray Technology*, 1999, **8**(1), 102.
21. Scardi, P., Cernuschi, F., Leoni, M. and Figari, A., Microstructure and Heat transfer phenomena in ceramic thermal barrier coatings. *J. Am. Ceram. Soc.*, 2001, **84**(4), 827–835.
22. Stille, U., Der Entmagnetisirungsfaktor und Entelektrisierungsfaktor fur Rotazionsellipsoide, Arch. *Elektrotech*, 1944, **38**, 91.
23. McLachlan, D. S., Equation for the conductivity of microscopic mixtures. *J. Phys. C: Solid State Phys*, 1986, **19**, 1339.
24. Mandelbrot, B. B., *Les objects fractals: forme, hasard et dimension*. Flammarion, Paris, 1975.
25. Mandelbrot, B. B., Passoja, D. and Paullay, A., The fractal character of fracture surfaces of metals. *Nature*, 1984, **158**, 721–722.
26. Mandelbrot, B. B., Self-affine fractal and fractal dimension. *Physica Scripta*, 1985, **32**, 257–260.
27. McPherson, R., A model for the thermal conductivity of plasma-sprayed ceramic coatings. *Thin Solid Films*, 1984, **112**, 89.
28. Bianchi, P., Cernuschi, F., Lorenzoni, L., Ahmaniemi, S., Vippola, M., Vuoristo, P. and Mäntylä, T., Thermophysical and Microstructural Characterisation of Modified Thick Yttria Stabilised Zirconia Thermal Barrier Coatings, in *Proceedings of "Materials for Advanced Power Engineering 2002"*, ed. J. Lecomte-Beckers, M. Carton, F. Schubert, P. J. Ennis, Schriften des Forschungszentrum Julich, 2002, pp. 449–463.
29. Ahmaniemi, S., Vippola, M., Vuoristo, P., Mantyla, T., Cernuschi, F. and Luterotti, L., Modified Thick Thermal Barrier Coatings, Part I: Microstructural Characterization, *J. Eur. Ceram. Soc.*, 2003 (submitted for publication).
30. Ahmaniemi, S., Vuoristo, P., Mäntylä, T., Cernuschi, F. and Lorenzoni, L., Modified thick thermal barrier coatings, part ii: thermophysical characterization, *J. Eur. Ceram. Soc.*, 2003 (submitted for publication).
31. Schwingel, D., Persson, C., Taylor, R., Johannesson, T. and Wigren, J., Thick thermal barrier coatings. *High Temp. High Press.*, 1995/1996, **27/28**(3), 273–282.
32. Leigh, S. and Berndt, C. C., Quantitative evaluation of void distributions within a plasma-sprayed ceramic. *J. Am. Ceram. Soc.*, 1999, **82**(1), 17–21.
33. Schlichting, K. W., Padture, N. P. and Klemens, P. G., Thermal conductivity of dense and porous yttria-stabilised zirconia. *J. Mater. Sci.*, 2001, **36**, 3003–3010.
34. Ilavsky, J., Long, G. G., Allen, A. J. and Berndt, C. C., Evolution of the void structure in plasma-sprayed YSZ deposits during heating. *Mater. Science and Engineering, A272*, 1999, 215–221.
35. Dutton, R., Wheeler, R., Ravichandran, K. S. and An, K., Effect of heat treatment on the thermal conductivity of plasma-sprayed thermal barrier coatings. *J. Thermal Spray Technol*, 2000, **9**(2), 204.
36. Thompson, J. A. and Clyne, T. W., The effect of heat treatment on the stiffness of zirconia top coats in plasma-sprayed TBCs. *Acta Mater.*, 2001, **49**, 1565–1575.